EARTH OBSERVATION AND GEOMATICS ENGINEERING
website: https://eoge.ut.ac.ir

# A quality assessment on the DEM matching-based RPC bias correction

**Hamed Afsharnia[1,2], Hossein Arefi[1]***

[1] School of Surveying and Geospatial Engineering, College of Engineering, University of Tehran, Tehran, Iran
[2] Department of Surveying Engineering, University of Zanjan, Zanjan, Iran

**Article history:**
Received: 25 February 2019, Received in revised form: 17 August 2019, Accepted: 4 September 2019

**ABSTRACT**

Rational polynomial coefficients delivered by satellite image vendors facilitate the geometric processing of images. However, compensating the inherent bias of these coefficients requires in-situ ground control collection. Existing global digital elevation models are an alternative for in-situ control data collection. In this regard, the well-known DEM matching technique can be applied for aligning the image-driven DEMs with the existing global elevation models. In this study, three image-driven DEMs were generated using a commercial programming application. The commercial software, similar to the majority of other software packages, performs epipolar resampling using vendor-provided RPCs before image matching. These generated DEMs were imported to the DEM matching technique and the estimated matching parameters were utilized for correcting the bias of RPCs on the ground. We showed that epipolar resampling with vendor-provided RPCs imposes some geometric distortions to the generated DEMs and therefore, estimated that DEM matching parameters cannot be employed for RPC bias correction. In two study areas, while the geopositioning accuracy after bias correction was improved 95.6% and 93.1% using the commercial software, we achieved 97.8% and 97.4% improvement using the programming.

**KEYWORDS**

Satellite stereo images
RPC bias correction
Digital Elevation Models
DEM matching

## 1. Introduction

High-Resolution Satellite Images (HRSIs) are among the primary sources of generating digital elevation models. The spatial resolution of these images ranges between 1m to 5m, and therefore, each image covers several square kilometers. HRSIs are supplied with Rational Polynomial Coefficients (RPCs).

Systematic errors are inherent in the RPCs (Toutin 2004, Aguilar & Nemmaoui et al. 2019). The complexity of these errors is different in each satellite. Also, regarding the acquired image data with a specific satellite, the magnitude of errors varies and should be corrected. Correction methods are called bias correction methods (Fraser & Dial et al. 2006) and may be described by a constant shift or constant shift and drift, and or by the affine transformation model (Tong & Liu et al. 2010). The parameters of these models are estimated using the ground control data.

The most commonly employed control data to estimate the parameters of the bias correction model are Ground Control Points (GCPs). In-situ collection of GCPs is a time- and energy-consuming task (Misra & Moorthi et al. 2015). Various techniques have been introduced as alternatives to direct the collection of GCPs.

Bias correction strategy can be designed for a single-image (Safdarinezhad & Mokhtarzade et al. 2016), the stereo image pairs (Teo & Huang 2013, Rastogi & Agrawal et al. 2015, Wu & Tang et al. 2015), or a block of images (d'Angelo & Reinartz 2012, Oh & Lee et al. 2013). DEM matching was first proposed by (Ebner & Müller 1986) for block adjustment of aerial photographs. Then, its complete mathematical relations were developed based on minimizing the sum of squares of vertical differences between two elevation models (Rosenholm & Torlegard 1987).

For generating the 3D stereo models, after conducting the image matching technique between the stereo image pair, the

* Corresponding author
E-mail addresses: hossein.arefi@ut.ac.ir (H. Arefi); afsharnia@ut.ac.ir, afsharnia@znu.ac.ir (H. Afsharnia)

DOI: 10.22059/eoge.2020.286773.1059

resulted matched points and vendor-provided RPCs are imported into the space intersection step. We named these stereo models as image-driven digital elevation models or simply as IDEMs.

In (d'Angelo & Schwind et al. 2009), the DEM matching method was performed on the satellite stereo images without describing the mathematical model of the matching. Also, sufficient assessments were not made in order to determine the efficiency of the method in linear array images. The complete expansion of the mathematical model of DEM matching for satellite imagery was performed by (Kim & Jeong 2010, Kim & Jeong 2011) based on the Rigorous Sensor Model (RSM).

As a consequence, if there is more than one image, the freely available global elevation models are applied as the alternative to the GCPs. These models can also be in the form of elevation profiles. For instance, (Rastogi & Agrawal et al. 2015) performed bias correction using the ICESat/GLAS laser profiles. In a similar work, these profiles have been utilized to improve the quality of 1:50000 map production from ZY-3 stereo images. An improvement in height precision from 5m to 3m was reported (Li & Tang et al. 2016).

In the present study, the approach proposed by Ebner and Müller was utilized to discover the bias of RPCs. Therefore, the 3D similarity transformation model was solved in the framework of the UTM coordinate system, and then, it was applied to the generated IDEMs. We focused on the effect of the IDEM generation procedure in the estimated parameters of the transformation model. The most employed pre-processing step in the IDEM generation algorithms is the epipolar resampling, generally using the vendor-provided RPCs (Alidoost & Azizi et al. 2015, Alizadeh Naeini & Fatemi et al. 2019). We designed a few scenarios to assess the effect of this big step in the DEM matching procedure. As a new achievement, we analyzed the results of epipolar resampling with vendor-provided RPCs in the geometric quality of generated IDEMs. In this regard, a popular software (PCI Geomatica) was used to generate two different IDEMs. Both IDEMs were generated based on the epipolar-resampled image pairs; one of them was resampled using the vendor-provided RPCs (PCIDEM) and the other one using the modified RPCs by GCPs (GCPDEM).

For a better assessment, we generated an IDEM without the epipolar resampling based on programming (MATDEM) to show the effect of resampling with biased RPCs in the results of no-GCP bias correction.

Section 2 introduces the collected materials and utilized mathematical models. The experimental results are reported in Section 3 and discussed in Section 4. Finally, the concluding remarks are presented in Section 5.

## 2. Materials and Methods

### 2.1. Study areas and data specifications

Two study areas in Iran were selected for performing the experiments. Each area consists of a pair of Cartosat-1 stereo images. The geographic locations of these areas are presented in Figure 1.

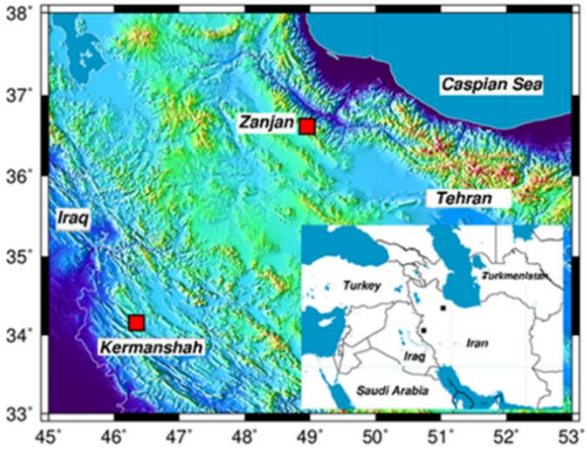


Figure 1. Geographic location of the two study areas

Table 1. Specifications of RDEM and IDEMs

| Elevation models | *SRTM V3 (RDEM)* | *MATDEM* | *PCIDEM* | *GCPDEM* |
|---|---|---|---|---|
| Data source | NASA Website (JPL. 2013) | Implemented program | PCI Geomatica software | PCI Geomatica software |
| Data format | Raster | Point cloud | Point cloud | Point cloud |
| Spatial resolution | 1 arcsecond | 0.5 arcseconds | 0.5 arcseconds | 0.5 arcseconds |

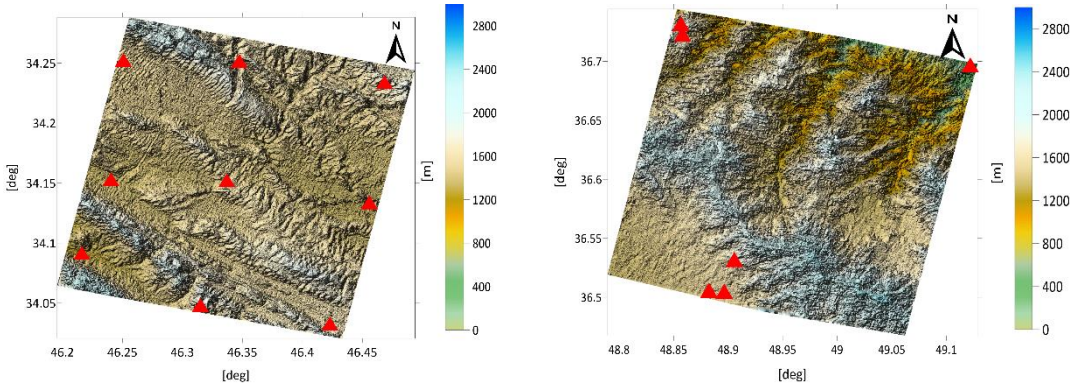


(a) MATDEM-Region-KA (b) MATDEM-Region-TA

Figure 2. Generated IDEMs for two study areas along with the position of GCPs on each IDEM. MATDEM is an IDEM generated by programming.

The image pairs were captured in 2008 from the Kalkosh region, located in Kermanshah Province and, in 2016, from the Tarom region of Zanjan Province, which we labeled them Region-KA and Region-TA, respectively.

The vendor-provided RPCs, in-situ collected GCPs, and 1-arcsecond SRTM data were available for both regions. According to previous studies (Varga & Bašić 2015, Santillan & Makinano-Santillan 2016), researchers have identified that the absolute vertical accuracy of SRTM data is higher than similar global DEMs. We used the SRTM data as a Reference DEM (RDEM) in the DEM matching step.

In order to discover the amount of bias in the RPCs, three IDEMs were generated using available input data. The first IDEM was generated using an implemented code called MATDEM without epipolar resampling. The generated IDEMs and the position of GCPs are shown in Figure 2.

The other two IDEMs were generated using the OrthoEngine module of PCI Geomatica software with and without the presence of GCPs, which were named GCPDEM and PCIDEM, respectively. The general specifications of the IDEMs and RDEM are listed in Table 1.

### 2.2. Geometric correction of satellite images

The most commonly used model for geometric correction of satellite images is the Rational Function Model (RFM). The RFM is written in the form of the ratio of third-order polynomials. This model is more straightforward than the RSM as it can be used without knowing orbital parameters and internal geometry of the sensor (Li & Niu et al. 2009).

The RFM, as well as some other mathematical models, such as the Direct Linear Transformation (DLT) model and the 2D affine model, have been proposed as an alternative to the RSM in most HRSIs. Since the coefficients of RFM in the form of RPCs are supplied with satellite images, it is the most widely used model for geometric correction of these images. The direct form of RFM equations are written as (Tao & Hu 2001):

$$L_n = \frac{P_1(\varphi_n, \lambda_n, h_n)}{P_2(\varphi_n, \lambda_n, h_n)}, S_n = \frac{P_3(\varphi_n, \lambda_n, h_n)}{P_4(\varphi_n, \lambda_n, h_n)} \quad (1)$$

$(L_n, S_n)$: Normalized image coordinates
$P_1, \dots, P_4$: Third-order polynomials
$(\varphi_n, \lambda_n, h_n)$: Normalized ground coordinates in the geodetic coordinate system

The general form of third-order polynomials are as follows:

$$P(\varphi_n, \lambda_n, h_n) = \sum_{m_1=0}^{3}\sum_{m_2=0}^{3}\sum_{m_3=0}^{3} a_k \varphi_n^{m_1} \lambda_n^{m_2} h_n^{m_3}; m_1 + m_2 + m_3 \le 3; k = 1:20 \quad (2)$$

$a_k$: Polynomial coefficients

Although the RFM does not address the source of geometric errors in the image, by using the terrain-independent method, its accuracy is approximately near to the RSM (Fraser & Dial et al. 2006, Topan & Oruc et al. 2014). Therefore, RFM is an appropriate alternative to the RSM (Jannati & Valadan Zoej et al. 2017).

The RPCs are estimated with the terrain-independent method by fitting the RFM equations to the direction of rays reconstructed using satellite ephemeris data. Satellite ephemeris data have some errors, the effect of which is propagated to the RPCs. Despite the high accuracy of fitting (Tao & Hu 2001), the lack of ground control information in the terrain-independent method causes the error of the ephemeris data to be propagated to the estimated RPCs (Pan & Tao et al. 2016). For this reason, there is an absolute error in these coefficients, which usually decreases by using GCPs. Fortunately, a significant amount of this error is systematic and it can be modeled (Teo 2011).

### 2.3. RPC bias correction approach

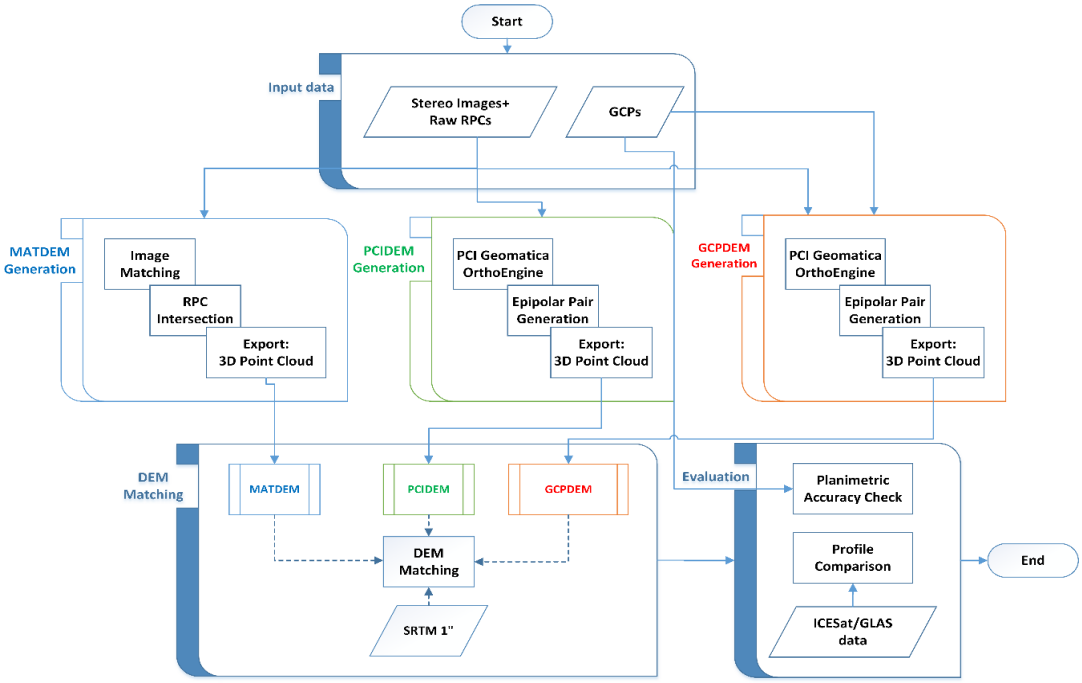


Figure 3. Study flowchart. Note that each IDEM is separately matched to the SRTM.

As mentioned in the introduction section, the first solution in reducing the bias of RPCs is the use of GCPs. The global elevation models that cover wide areas can substitute GCPs. There cannot be a high expectation from alternative methods; however, by considering applications that do not require high accuracies, it is reasonable to utilize these alternatives.

After generating an IDEM from a pair of satellite images, it can be matched with a global elevation model (e.g., RDEM). Although RDEMs usually have a low resolution, the horizontal accuracy of these models is better than that of IDEMs derived from Cartosat-1 images (Bagheri & Schmitt et al. 2018). As a result, after matching two elevation models, a product is achieved with a better spatial resolution compared to the RDEM and accuracy higher than that of the IDEM. This process, without the need for GCP collection, reduces the bias of RPCs on the final product.

The flowchart of the overall progress of this study is presented in Figure 3. The process starts with the generation of IDEMs. Then, each IDEM is individually matched to the RDEM and the transformation parameters are calculated for each DEM. Finally, the quality of DEM matching is evaluated using the collected GCPs.

### 2.3.1 Mathematical model of DEM matching

Various mathematical models for DEM matching have been used in similar investigations. For example, in (Sedaghat & Alizadeh Naeini 2018), three different mathematical models, including the 3D rigid model, the 3D similarity transformation, and the 3D affine model, were applied. However, according to (Kim & Jeong 2011), the 3D similarity transformation is sufficient for the matching of the elevation models extracted from a pair of linear array satellite images.

The formation of mathematical equations for matching the elevation models requires the introduction of data structures and their coordinate systems. IDEMs in the form of an irregular point cloud, without a need for gridding and interpolation, are directly matched to the global DEM with a regular structure. The essential changes are the use of the UTM projection system for the point cloud and SRTM data, as well as the transformation of the SRTM data from EGM96 to WGS84 to unify the height datum of the two elevation models.

In this study, a DEM matching method was adopted to solve all the transformation parameters in an iterative process simultaneously. This method was implemented based on Ebner's model (Ebner & Müller 1986) which itself is based on the 3D similarity transformation as follows:

$$V_Z = -\left(\frac{\partial Z_r}{\partial E}\right)dE_o - \left(\frac{\partial Z_r}{\partial N}\right)dN_o + dZ_o + \left(N + \left(\frac{\partial Z_r}{\partial N}\right)Z\right)\mathrm{d}\Omega + \left(-E - \left(\frac{\partial Z_r}{\partial E}\right)Z\right)\mathrm{d}\Phi + \left(\left(\frac{\partial Z_r}{\partial E}\right)N - \left(\frac{\partial Z_r}{\partial N}\right)E\right)d\,\mathrm{K} + \left(Z - \left(\frac{\partial Z_r}{\partial E}\right)E - \left(\frac{\partial Z_r}{\partial N}\right)N\right)dm - \left[Z_a(E,N) - Z\right] \quad (3)$$

$(E, N, Z)$: UTM coordinates (Easting, Northing, and ellipsoid height) of the selected point in the point cloud
$Z_r$: Interpolated height from the RDEM
$[dE_o, dN_o, dZ_o, d\Omega, d\Phi, dK, dm]$: Differential values of the 3D similarity transformation parameters used for DEM matching
$n$: Number of selected points

Due to the large volume of the generated point cloud as IDEM, some well-distributed points are selected (named as selected points). The observation equations for selected points are written based on equation (3) and each point adds an equation to this observation equation system. Substituting $G_E = \partial Z_r/\partial E$ and $G_N = \partial Z_r/\partial N$ in equation (3), the matrix form of this equation is expressed as follows:

$$\begin{bmatrix} Z_1 - Z_{r_1} \\ \vdots \\ Z_n - Z_{r_n} \end{bmatrix} = \begin{bmatrix} -G_{E_1} & -G_{N_1} & 1 & (N_1 + G_{N_1} Z_1) & (-E_1 - G_{E_1} Z_1) & (G_{E_1} N_1 - G_{N_1} E_1) & (Z_1 - G_{E_1} E_1 - G_{N_1} N_1) \\ \vdots & \vdots & \vdots & \vdots & \vdots & \vdots & \vdots \\ -G_{E_n} & -G_{N_n} & 1 & (N_n + G_{N_n} Z_n) & (-E_n - G_{E_n} Z_n) & (G_{E_n} N_n - G_{N_n} E_n) & (Z_n - G_{E_n} E_n - G_{N_n} N_n) \end{bmatrix} \begin{bmatrix} dE_o \\ dN_o \\ dZ_o \\ d\Omega \\ d\Phi \\ d\mathrm{K} \\ dm \end{bmatrix} \quad (4)$$

$G_E, G_N$: Interpolated directional gradients (slopes) from the RDEM

*1,…,n* indices: represents the selected point number

After estimating the transformation parameters, these parameters are applied to all selected points at the end of each iteration, as follows:

$$\begin{bmatrix} E \\ N \\ Z \end{bmatrix}^{j+1} = (1+dm) \begin{bmatrix} 1 & -dK & d\Phi \\ dK & 1 & -d\Omega \\ -d\Phi & d\Omega & 1 \end{bmatrix} \begin{bmatrix} E \\ N \\ Z \end{bmatrix}^{j} + \begin{bmatrix} dE_o \\ dN_o \\ dZ_o \end{bmatrix} \quad (5)$$

$j$: Iteration number of the DEM matching procedure

Directional gradients are computed from RDEM in the position of selected points. We know that, at the end of each iteration of DEM matching, the position of all selected points is updated. Therefore, directional gradients should be computed in each iteration.

Although the differential values are applied to the IDEM in each iteration, the total values of these parameters in all iterations are reported as the final transformation parameters. As a result, the mathematical model of the RPC bias compensation in the ground space can be written as:

$$\begin{aligned} \Delta E &= mE^{\,j} - KN^{\,j} + \Phi Z^{\,j} + E_o \\ \Delta N &= KE^{\,j} + mN^{\,j} - \Omega Z^{\,j} + N_o \\ \Delta Z &= -\Phi E^{\,j} + \Omega N^{\,j} + mZ^{\,j} + Z_o \end{aligned} \quad (6)$$

### 2.4. Generation of MATDEM

In all steps of the MATDEM generation (except in the seed point generation step to start the precise image matching process), any corrections to the geometric properties of stereo images should be avoided. In this way, the bias in the vendor-provided RPCs is propagated to the generated DEM. If the corrections are applied, the actual effect of RPC bias in the final MATDEM could not be discovered adequately. In summary, no specific geometric corrections should be performed before DEM matching. For this purpose, an image matching strategy is first implemented.

#### 2.4.1. Image matching strategy

The desired specifications for IDEM determine the image matching method. Here, a dense matching method is needed. The Least-Squares Image Matching (LSM) method, as an area-based method, has the potential to achieve high precision and is mainly used for increasing the accuracy of other matching methods (Sohn & Park et al. 2005). However, the LSM method has a small pull-in-range and it is possible to get into the local minima of the correlation function, which in turn reduces the reliability of the results. Therefore, it is essential to produce the appropriate seed points located within the small convergence radius of the LSM. Here, the seed points were obtained using a coarse matching method that incorporates the vendor-provided RPCs and SRTM elevation model in the image matching procedure.

The seed points are extracted using the coarse matching method. In this regard, a regular grid should be assumed on the first image, and the grid points are transferred to the surface of the SRTM model using the RPCs of this image. Then, the grid points are transferred to the second image using the RPCs of this image. Finally, we apply a 1D search using the cross-correlation method for finding the best match of each grid point. The corresponding points extracted from the coarse matching method are named as seed points.

After completing the coarse matching, the precise matching is performed with the LSM method. As mentioned in the introduction section, the least-squares technique is considered to improve the position of the seed points. The mathematical equations of this technique have been presented in the literature (Gruen 1985, Zhang 2005). The LSM is performed in the image domain and is based on the gray levels of image patches (windows) taken from stereo images. The dimensions of a square patch are considered to be 35 by 35 pixels based on the auto-correlation function of the template patch (Afsharnia & Arefi et al. 2017).

#### 2.4.2. Space intersection using RFM

The corresponding points obtained from precise matching, along with the RPC data of the stereo images are involved in the generation of MATDEM. The space intersection equations based on the direct RFM have been mentioned in numerous references (Tao & Hu 2001, Fraser & Hanley 2003). The output of space intersection is a 3D point cloud in a ground space named MATDEM.

Table 2. The reference ellipsoids and height layers of the experimental data; in the implementation process, all data should be transformed into a standard coordinate system.

| Item | Height datum | Reference ellipsoid |
|---|---|---|
| IDEMs | WGS84 ellipsoid | WGS84 |
| SRTM (RDEM) | EGM96 geoid | WGS84 |
| GCPs | WGS84 ellipsoid | WGS84 |
| Common frame | WGS84 ellipsoid | WGS84 |

2.4.3. Blunder removal

In general, the geometric quality of MATDEM directly depends on the image matching quality. The remained false matches in the corresponding points lead to making some blunders in MATDEM. Therefore, a process was considered for identifying and eliminating the systematic blunders mentioned as follows:

I. Determining a threshold for the number of LSM iterations to eliminate the points in which the convergence has not been achieved.

II. Increasing the dimensions of the matching window if the LSM equations are not converged (which increases the radiometric content of the image window and consequently the probability of the convergence).

III. Removing the blunders of the space intersection. Based on the two criteria, the number of iterations and the residual values of space intersection, some of the generated ground points were eliminated. The predefined threshold for the number of iterations was 2, and the residuals that were not consistent with the remaining residuals were removed. Since the standard deviation of the space intersection with the vendor-provided RPC data was small (sigma is about 1.5 pixels), the residual values far from the mean of the residual vector (larger than 3*sigma) indicated a false matching in the previous step.

IV. Generating a temporary DEM from the extracted point cloud by applying the median filter and comparing each point with the surface of this temporary DEM. In this step, the blunders are identified and eliminated from the point cloud.

## 3. Experimental results

Different scenarios were considered to discover the errors inherent in the vendor-provided RPCs of the stereo pair. These scenarios were designed based on IDEM generation strategies. For each study area, we generated three different IDEMs, namely MATDEM, PCIDEM, and GCPDEM. The introduced DEM matching method in Section 2 was applied for all of these IDEMs and then, using the control data, we evaluated the impact of the IDEM generation strategy in the bias correction procedure.

Each input data is defined in a specific coordinate frame, which must be transformed into standard frames. The reference ellipsoids and height layers of these datasets are given in Table 2. In the last row of the table, the selected standard frame is introduced.

The conversion of heights from EGM96/EGM2008 to a WGS84 ellipsoid was easily achieved by considering the value of geodetic height at each point. The DEM matching procedure is performed after bringing all data to the standard reference frame. The convergence graphs of DEM matching are presented separately in Figures 4 and 5. These graphs were related to the 3D similarity transformation.

The values of transformation parameters in different scenarios are presented in Table 3. The larger parameters indicated more significant errors in the vendor-provided RPCs.

Table 3. Estimated parameters of DEM matching in different scenarios. MATDEMs were generated by programming, and PCIDEMs and GCPDEMs were generated using the PCI Geomatica software with and without GCP, respectively.

| Dataset | Scenario | $Xo$ [m] | $Yo$ [m] | $Zo$ [m] | $\Omega$ [sec] | $\phi$ [sec] | $K$ [sec] | $1+m$ |
|---|---|---|---|---|---|---|---|---|
| Region-KA | PCIDEM | 152.2 | -256.9 | 13.6 | -84.7 | -138.1 | -127.4 | 0.9999 |
| | MATDEM | 166.2 | -255.0 | 12.1 | -32.5 | -72.2 | -59.2 | 0.9998 |
| | GCPDEM | 0.8 | -2.7 | -3.2 | -10.7 | 1.9 | -26.4 | 0.9999 |
| Region-TA | PCIDEM | 71.3 | -1019.1 | -422.3 | -87.2 | -70.0 | -253.1 | 0.9977 |
| | MATDEM | 3.3 | -1008.0 | -413.9 | 61.7 | 107.2 | -250.2 | 0.9997 |
| | GCPDEM | -2.4 | 0.8 | 5.3 | 47.8 | 50.6 | -16.7 | 1.0000 |

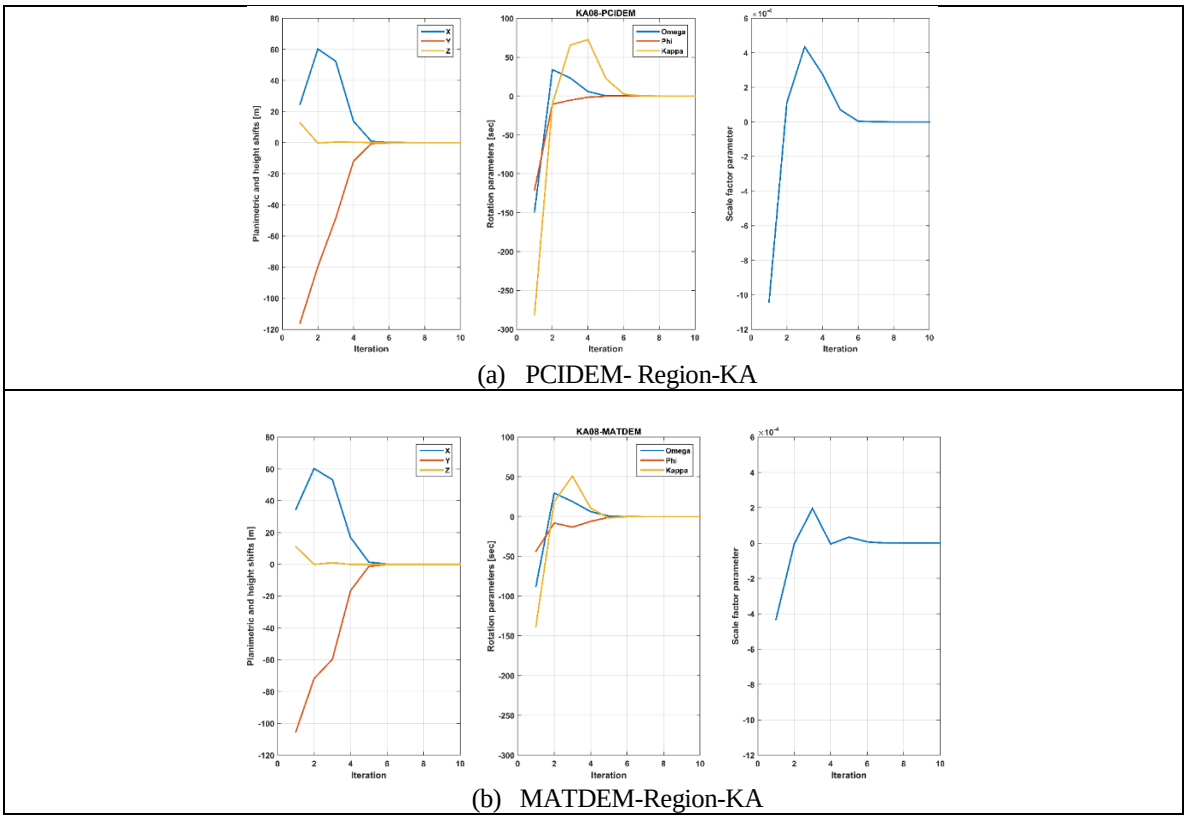


(a) PCIDEM- Region-KA

(b) MATDEM-Region-KA

Figure 4. Convergence graphs of DEM matching for Region-KA

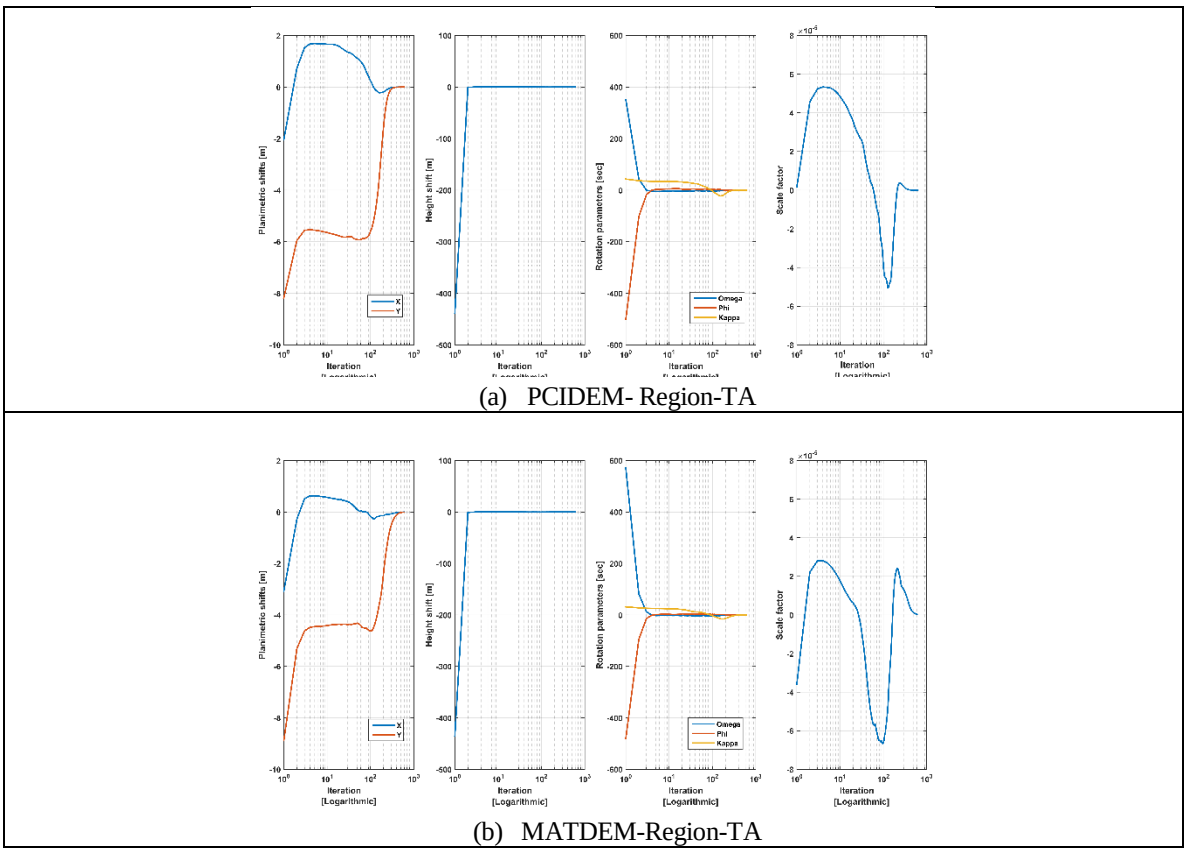


(a) PCIDEM- Region-TA

(b) MATDEM-Region-TA

Figure 5. Convergence graphs of DEM matching for Region-TA. In this dataset, matching was converged in 600 iterations and for better presentation, the graphs were plotted on the logarithmic scale.

### 3.1. The optimal number of selected points

The available GCPs examined the effect of the number of selected points in the results of bias correction. We tested five different sampling rates from the generated dense point cloud in Region-KA, and then we computed the achieved horizontal accuracy after bias correction. With the sampling rate of 1/100, the best accuracy was reached and by increasing the sampling rate, no further improvements were observed (as shown in Figure 6). The selected points are distributed uniformly and randomly.

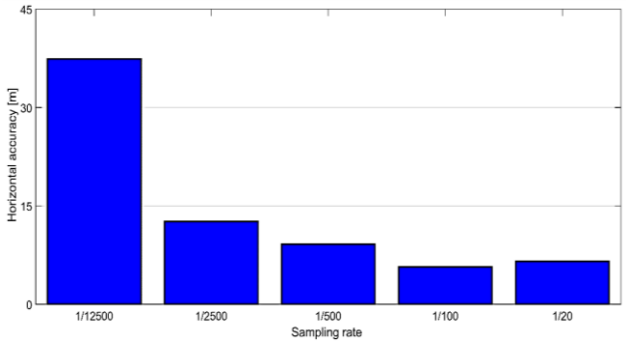


Figure 6. The horizontal accuracy derived from the differences between the longitudes and the latitudes of GCPs and their corresponding bias-corrected points in Region-KA.

### 3.2. Quality assessment

The evaluation of DEM matching was carried out in three ways. One external and two internal evaluations were considered as follows:

- an external evaluation using GCPs
- visual comparison by generating height difference maps
- and, statistical analyses using height difference histograms

#### 3.2.1. Accuracy criteria

If a normal distribution is presumed for the height difference vector, the following criteria can be presented in the quality evaluation of DEM matching:

$$RMSE = \sqrt{\frac{1}{n}\sum_{i=1}^{n}\Delta Z_i^{\,2}} \tag{7}$$

$$Mean\,error = \overline{\Delta Z} = \frac{1}{n}\sum_{i=1}^{n}\Delta Z_i \tag{8}$$

$$Std\,(LE\,68) = \sqrt{\frac{1}{(n-1)}\sum_{i=1}^{n}\left(\Delta Z_i - \overline{\Delta Z}\right)^2} \tag{9}$$

$\Delta Z_i$: Height difference between the IDEM and the RDEM at the point $i$
$RMSE$: RMSE of the $\Delta Z$ vector based on the 68% confidence interval
$Std$: Standard deviation of height differences around the $Mean\ error$ based on the 68% confidence interval

In addition, a robust criterion should be created that would not be sensitive to outlier elements. The Normalized Median Absolute Deviation ($NMAD$) is a robust estimator expressed as follows (Höhle & Höhle 2009):

$$NMAD = 1.4826 \times median_i\left(\left|\Delta Z_i - median\left(\Delta Z\right)\right|\right) \tag{10}$$

In the following, the details of each evaluation and achieved results are presented.

Table 4. Statistical information on the difference between bias-corrected and GPS coordinates

| Dataset | Item | Scenario | mean [m] | \|max\| [m] | RMS [m] | RMS [pixel] | NMAD [m] |
|---|---|---|---|---|---|---|---|
| Region-KA | *Longitude* | PCIDEM | -13.0 | 20.6 | 14.0 | 5.6 | - |
| | | MATDEM | 0.2 | 3.6 | 2.3 | 0.9 | - |
| | *Latitude* | PCIDEM | 4.2 | 9.4 | 5.1 | 2.0 | - |
| | | MATDEM | 6.4 | 11.5 | 7.3 | 2.9 | - |
| | *Height* | PCIDEM | -0.3 | 10.2 | 4.7 | - | 4.2 |
| | | MATDEM | -1.4 | 9.1 | 3.7 | - | 2.4 |
| Region-TA | *Longitude* | PCIDEM | 54.4 | 73.6 | 57.0 | 22.8 | - |
| | | MATDEM | -8.3 | 33.3 | 18.6 | 7.4 | - |
| | *Latitude* | PCIDEM | 3.1 | 49.4 | 38.8 | 15.5 | - |
| | | MATDEM | 12.9 | 29.2 | 17.9 | 7.2 | - |
| | *Height* | PCIDEM | -1.4 | 12.8 | 10.3 | - | 10.0 |
| | | MATDEM | -0.9 | 6.8 | 3.7 | - | 1.7 |

3.2.2. The visual comparison

The visual comparison illustrated in Figure 7 shows the difference maps before and after DEM matching and also provides a basis for interpretations that cannot be performed by statistical analysis.

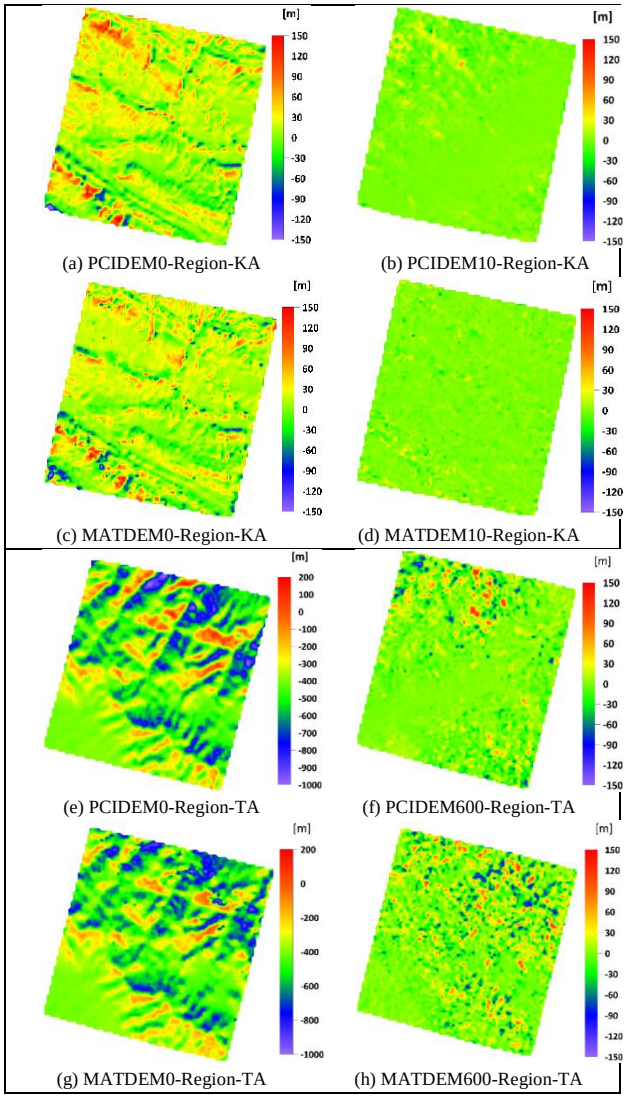


Figure 7. Height difference maps between IDEMs and their corresponding RDEM before and after conducting the DEM matching step in different scenarios. The numbers at the end of each IDEM's name show the number of iterations. MATDEMs were generated by programming and PCIDEMs were generated using the PCI Geomatica software.

3.2.3. Histogram analysis

The main objective of DEM matching methods is to reduce the vertical distance between two DEMs by applying the suitable geometric transformation. As a result, the histogram of height differences at the end of iterations could be an internal criterion for assessing the quality of matching. The histograms of height differences are shown in Figure 8.

It is not possible to analyze the quality of DEM matching only by considering the histograms and the height difference maps. Hence, the horizontal and altimetric control data have been used for a reliable analysis.

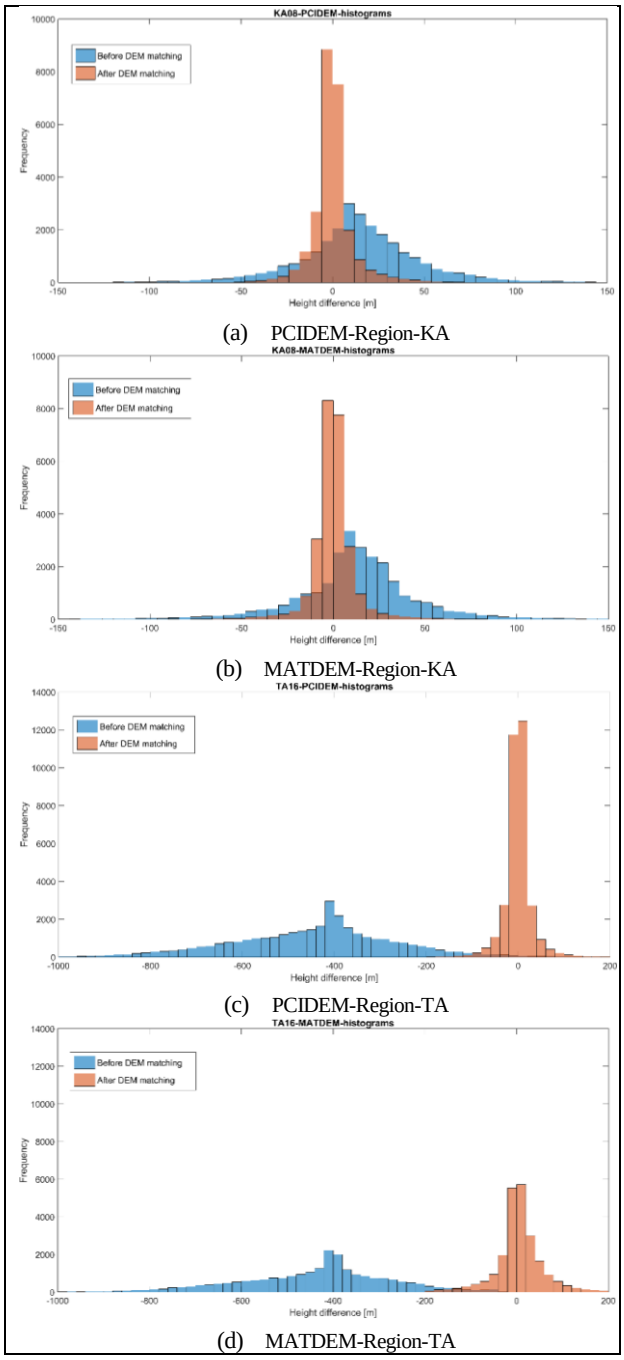


Figure 8. Histograms of height differences between IDEMs and their corresponding RDEM before and after DEM matching step in different scenarios.

**3.3. Accuracy assessment using the GCPs**

As mentioned in Section 2, a few GCPs measured by the differential GPS technique were collected from the study areas (9 GCPs for Region-KA and 6 GCPs for Region-TA). In the PCIDEMs, the GCPs were introduced as checkpoints to the software. In the case of MATDEMs, the RF derived

coordinates of points in the ground space were calculated using vendor-provided RPCs and the image coordinates of GCPs. Then, the 3D similarity transformation (estimated from the DEM matching) was applied to these RF-derived coordinates to achieve the bias-corrected coordinates. Finally, we calculated the horizontal and vertical accuracies by comparing the bias-corrected and in-situ measured coordinates. These accuracies are presented in Table 4.

As a comparison, we considered two similar types of research, both of which selected Cartosat-1 stereo images for evaluating their proposed method of bias correction. In the first research conducted in region-KA (Alidoost & Azizi et al. 2015), the epipolar resampling technique was used to have a robust, dense image matching. After bias correction of RPCs by SRTM in 9 GCPs, the evaluation showed an accuracy of -69.4±15.1m and 7.9±9.1m in X (longitude) and Y (latitude) coordinates, respectively. As seen in Table 4, we achieved an accuracy of 0.2±2.3m and 6.4±7.3m for these coordinates. There is a significant difference in RMSE values of longitude coordinate which can be attributed to epipolar resampling before DEM generation in their research.

In the second research (Alizadeh Naeini & Fatemi et al. 2019), the IDEMs were generated for two study areas using the PCI Geomatica software. A proposed 2.5D DEM matching procedure implemented bias correction with SRTM DEM, and in the evaluation step, only the vertical accuracy was assessed using a high-resolution reference DEM. While we achieved a vertical accuracy of -1.4±3.7m and -0.9±3.7m for two study areas, they reported 2.0±6.3m and -5.0±5.7m for their selected study areas. The lower vertical accuracy of their research could be related to the epipolar resampling with the vendor-provided RPCs.

## 4. Discussion

Based on the histograms in Figure 8, the output of the commercial software (PCIDEM) was better matched to the RDEM than the output of the implemented program (MATDEM). This is because the frequency of histogram around zero is more significant in the PCIDEM case for both datasets.

Unlike what was observed in histogram analysis, the horizontal accuracy for PCIDEM and MATDEM cases are 14.9m and 7.6m for the dataset of Region-KA and 69.0m and 18.3m for that of Region-TA, respectively. Also, the vertical accuracies in PCIDEMs are 4.7m and 10.3m for the datasets of Region-KA and Region-TA, respectively, while in MATDEMs it is 3.7m for both datasets. These results mean that after bias correction, MATDEMs are significantly more accurate than PCIDEMs.

To explain the reasons for these results, we should consider IDEM generation procedures in different scenarios. In the generation of MATDEM, the vendor-provided RPCs were utilized only at the space intersection. However, in PCIDEM generation, in addition to space intersection, these RPCs were used to epipolar resampling of image pairs. Thus, we can conclude that the bias in the RPCs caused a geometric distortion in parallax values of the generated epipolar pairs, and this distortion was also propagated to the generated PCIDEMs.

By looking at the transformation parameters in Table 3, it is clear that the transformation parameters differ significantly in the MATDEM and PCIDEM cases. As a result, it can be concluded that the low accuracy of PCIDEMs is due to the epipolar resampling with uncorrected RPCs because epipolar resampling is a necessary step before DEM generation in the PCI Geomatica software.

## 5. Conclusion

In order to modify the bias of vendor-provided RPCs, a global elevation model was used as an alternative for in-situ collected GCPs. First, an irregular point cloud was extracted from the stereo images (IDEM). Each point in the IDEM was produced using the RFM equations and vendor-provided RPCs. Therefore, it has the RF-derived coordinates and we assume that the bias contained in the RPCs was propagated to the RF-derived coordinates. Then, using the DEM matching method, we attempted to match this IDEM to a reference global DEM (RDEM). The estimated transformation parameters of DEM matching were used for bias correction of RPCs.

We designed three scenarios to assess the effect of IDEM generation on bias correction of RPCs and evaluated them on two study areas. The experiment was performed on two IDEMs that were generated using the PCI Geomatica software with and without GCPs (GCPDEM and PCIDEM) and on a generated IDEM using an implemented program (MATDEM). After evaluating the results using the control points and control profiles, it was concluded that MATDEM achieves more accurate results than PCIDEM. As a reason, it can be stated that epipolar resampling of stereo image pairs using vendor-provided RPCs in the PCI Geomatica software before DEM generation causes some distortion in the depths extracted from these images. Thus, the transformation parameters estimated in the DEM matching procedure for PCIDEM could not be considered for bias correction of RPCs.

In recent years, the majority of image matching algorithms used epipolar resampling as a pre-processing step. In this research, we showed that if the vendor-provided RPCs were used in the epipolar resampling step, the global elevation models could not be an alternative for GCPs in bias correction of the RPCs.

**Acknowledgement**

We thank the data provider, Iranian national geographic organization. Special thanks are given to the anonymous reviewers for their careful reading and helpful suggestions.

**References**


Afsharnia, H., H. Arefi, & M. A. Sharifi (2017). "Optimal Weight Design Approach for the Geometrically-Constrained Matching of Satellite Stereo Images." *Remote Sensing* 9(9): 965.

Aguilar, M. A., A. Nemmaoui, F. J. Aguilar, & R. Qin (2019). "Quality assessment of digital surface models extracted from WorldView-2 and WorldView-3 stereo pairs over different land covers." *GIScience & remote sensing* 56(1): 109-129.

Alidoost, F., A. Azizi, & H. Arefi (2015). "The Rational Polynomial Coefficients Modification Using Digital Elevation Models." *The International Archives of Photogrammetry, Remote Sensing and Spatial Information Sciences* 40(1): 47.

Alizadeh Naeini, A., S. B. Fatemi, M. Babadi, S. M. J. Mirzadeh, & S. Homayouni (2019). "Application of 30-meter global digital elevation models for compensating rational polynomial coefficients biases." *Geocarto International*: 1-16.

Bagheri, H., M. Schmitt, & X. X. Zhu (2018). "Fusion of TanDEM-X and Cartosat-1 elevation data supported by neural network-predicted weight maps." *ISPRS journal of photogrammetry and remote sensing* 144: 285-297.

d'Angelo, P., & P. Reinartz (2012). "DSM based orientation of large stereo satellite image blocks." *Int. Arch. Photogramm. Remote Sens. Spatial Inf. Sci* 39(B1): 209-214.

d'Angelo, P., P. Schwind, T. Krauss, F. Barner, & P. Reinartz (2009). Automated DSM based georeferencing of Cartosat-1 stereo scenes. *ISPRS Hannover Workshop: High-Resolution Earth Imaging for Geospatial Information*.

Ebner, H., & F. Müller (1986). "Processing of digital three-line imagery using a generalized model for combined point determination." *Photogrammetria* 41(3): 173-182.

Fraser, C. S., G. Dial, & J. Grodecki (2006). "Sensor orientation via RPCs." *ISPRS journal of Photogrammetry and Remote Sensing* 60(3): 182-194.

Fraser, C. S., & H. B. Hanley (2003). "Bias compensation in rational functions for IKONOS satellite imagery." *Photogrammetric Engineering & Remote Sensing* 69(1): 53-57, 0099-1112.

Gruen, A. (1985). "Adaptive least squares correlation: a powerful image matching technique." South African Journal of Photogrammetry, *Remote Sensing and Cartography* 14(3): 175-187.

Höhle, J., & M. Höhle (2009). "Accuracy assessment of digital elevation models by means of robust statistical methods." *ISPRS Journal of Photogrammetry and Remote Sensing* 64(4): 398-406.

Jannati, M., M. J. Valadan Zoej, & M. Mokhtarzade (2017). "A Knowledge-Based Search Strategy for Optimally Structuring the Terrain Dependent Rational Function Models." *Remote Sensing* 9(4): 345.

JPL., N. (2013). NASA Shuttle Radar Topography Mission Global 1 arc second. https://lpdaac.usgs.gov/products/srtmgl1v003/ [Data set]. N. L. DAAC.

Kim, T., & J. Jeong (2010). "Precise mapping of high resolution satellite images without ground control points." *International Archives of Photogrammetry, Remote Sensing and Spatial Information Sciences* 38(5).

Kim, T., & J. Jeong (2011). "DEM matching for bias compensation of rigorous pushbroom sensor models." ISPRS journal of photogrammetry and remote sensing 66(5): 692-699.

Li, G., X. Tang, X. Gao, H. Wang, & Y. Wang (2016). "ZY-3 Block adjustment supported by glas laser altimetry data." *The Photogrammetric Record* 31(153): 88-107.

Li, R., X. Niu, C. Liu, B. Wu, & S. Deshpande (2009). "Impact of imaging geometry on 3D geopositioning accuracy of stereo IKONOS imagery." *Photogrammetric Engineering & Remote Sensing* 75(9): 1119-1125.

Misra, I., S. M. Moorthi, D. Dhar, & R. Ramakrishnan (2015). "A Unified Software Framework for Automatic Precise Georeferencing of Large Remote Sensing Image Archives." *Procedia Computer Science* 46: 812-819.

Oh, J., C. Lee, & D. C. Seo (2013). "Automated HRSI georegistration using orthoimage and SRTM: Focusing KOMPSAT-2 imagery." *Computers & geosciences* 52: 77-84.

Pan, H., C. Tao, & Z. Zou (2016). "Precise georeferencing using the rigorous sensor model and rational function model for ZiYuan-3 strip scenes with minimum control." *ISPRS Journal of Photogrammetry and Remote Sensing* 119: 259-266.

Rastogi, G., R. Agrawal, & Ajai (2015). "Bias corrections of CartoDEM using ICESat-GLAS data in hilly regions." *GIScience & Remote Sensing* 52(5): 571-585.

Rosenholm, D., & K. Torlegard (1987). "Three-dimensional absolute orientation of stereo models using digital elevation models." *Photogrammetric engineering and remote sensing* 54: 1385-1389.

Safdarinezhad, A., M. Mokhtarzade, & M. J. V. Zoej (2016). "Coregistration of satellite images and airborne lidar data through the automatic bias reduction of rpcs." *IEEE Journal of Selected Topics in Applied Earth Observation and Remote Sensing*, vol. 1, no. 5.

Santillan, J., & M. Makinano-Santillan (2016). "Vertical Accuracy Assessment of 30-M Resolution Alos, Aster, and SRTM Global DEMs over Northeastern Mindanao, Philippines." *International Archives of the Photogrammetry, Remote Sensing & Spatial Information Sciences* 41.

Sedaghat, A., & A. Alizadeh Naeini (2018). "DEM orientation based on local feature correspondence with

global DEMs." *GIScience & Remote Sensing* 55(1): 110-129.

Sohn, H. G., C. H. Park, & H. Chang (2005). "Rational function model- based image matching for digital elevation models." *The Photogrammetric Record* 20(112): 366-383.

Tao, C. V., & Y. Hu (2001). "A comprehensive study of the rational function model for photogrammetric processing." *Photogrammetric engineering and remote sensing* 67(12): 0099-1112.

Teo, T.-A. (2011). "Bias compensation in a rigorous sensor model and rational function model for high-resolution satellite images." *Photogrammetric Engineering & Remote Sensing* 77(12): 1211-1220.

Teo, T.-A., & S.-H. Huang (2013). "Automatic co-registration of optical satellite images and airborne LiDAR data using relative and absolute orientations." *IEEE Journal of Selected Topics in Applied Earth Observations and Remote Sensing* 6(5): 2229-2237.

Tong, X., S. Liu, & Q. Weng (2010). "Bias-corrected rational polynomial coefficients for high accuracy geo-positioning of QuickBird stereo imagery." *ISPRS Journal of Photogrammetry and Remote Sensing* 65(2): 218-226.

Topan, H., M. Oruc, T. Taskanat, & A. Cam (2014). "Combined efficiency of RPC and DEM accuracy on georeferencing accuracy of orthoimage: Case study with Pléiades panchromatic mono image." *IEEE Geoscience and Remote Sensing Letters* 11(6): 1148-1152.

Toutin, T. (2004). "Geometric processing of remote sensing images: models, algorithms and methods." *International journal of remote sensing* 25(10): 1893-1924.

Varga, M., & T. Bašić (2015). "Accuracy validation and comparison of global digital elevation models over Croatia." *International journal of remote sensing* 36(1): 170-189.

Wu, B., S. Tang, Q. Zhu, K.-y. Tong, H. Hu, & G. Li (2015). "Geometric integration of high-resolution satellite imagery and airborne LiDAR data for improved geopositioning accuracy in metropolitan areas." *ISPRS Journal of Photogrammetry and Remote Sensing* 109: 139-151.

Zhang, L. (2005). "Automatic digital surface model (DSM) generation from linear array images." *Ph.D Dissertation, Mitteilungen- Institut fur Geodasie und Photogrammetrie an der Eidgenossischen Technischen Hochschule Zurich*: 0252-9335.